THE JOURNAL OF PHYSICAL CHEMISTRY A
A JOURNAL OF THE AMERICAN CHEMICAL SOCIETY

pubs.acs.org/JPCA Article

Destructive Processing of Silicon Carbide Grains: Experimental Insights into the Formation of Interstellar Fullerenes and Carbon Nanotubes

Published as part of The Journal of Physical Chemistry virtual special issue "10 Years of the ACS PHYS Astrochemistry Subdivision".

Jacob J. Bernal,* Thomas J. Zega, and Lucy M. Ziurys

Cite This: https://doi.org/10.1021/acs.jpca.2c01441 Read Online

ACCESS | Metrics & More | Article Recommendations

ABSTRACT: The detection of the fullerenes C_{60} and C_{70} in the interstellar medium (ISM) has transformed our understanding of chemical complexity in space. These discoveries also raise the possibility for the presence of even larger molecules in astrophysical environments. Here we report in situ heating of analog silicon carbide (SiC) presolar grains using transmission electron microscopy (TEM). These heating experiments are designed to simulate the temperature conditions occurring in post-AGB stellar envelopes. Our experimental findings reveal that heating the analog SiC grains to the point of decomposition initially yields hemispherical C_{60}-sized nanostructures, with five- and six-membered rings, which transform into multiwalled carbon nanotubes (MWCNTs) if held isothermally >2 min. These MWCNTs are certainly larger than any of the currently observed interstellar fullerene species, both in overall size and number of C atoms. These experimental simulations suggest that such MWCNTs are likely to form in post-AGB circumstellar material, where the structures, along with the smaller fullerenes, are subsequently injected into the ISM.

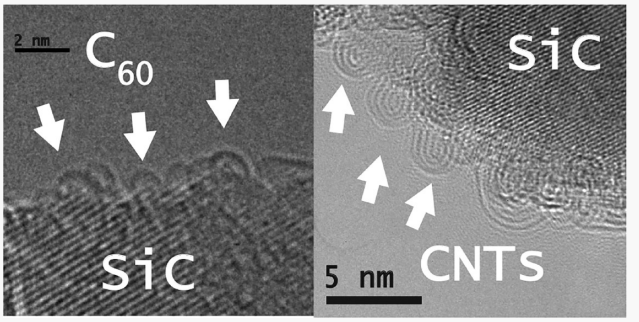

INTRODUCTION

Establishing a mechanism for the synthesis of fullerenes in the interstellar medium (ISM) has been a challenge for astrochemistry (e.g., ref 1). Over the past decade, observations have shown that both C_{60} and C_{70} are present in planetary nebulae and other circumstellar environments (e.g., refs 2−4), as well as in diffuse clouds.[5] It has been shown that C_{60}^+ also occurs in diffuse gas and accounts for several of the diffuse interstellar bands, or "DIBs" (e.g., 6−8). Despite the increased identifications, a facile mechanism that can readily cohere sp^2-hybridized carbon atoms together to form thermodynamically stable nanofragments and nanostructures in environments that are rich in hydrogen and other elements under typical astrophysical conditions has yet to be proposed.[3] "Bottom-up" formation processes are thought to be unlikely, as time scales are too long to build a 60 to 70 atom molecule given typical interstellar densities and temperatures (e.g., ref 5). "Top-down" synthesis seems to be more viable, with either hydrogenated amorphous carbon ("HACs") or polycyclic aromatic hydrocarbons (PAHs), as the starting materials (e.g., ref 9).

Experimental work shows that fullerene-like structures can be generated in HACs (e.g., refs 10 and 11). Furthermore, studies by Tielens, Berné, and collaborators (e.g., refs 5, 9, 12, and 13) suggest that PAHs may be a route to C_{60} by a series of processes involving dehydrogenation, folding, and shrinking. However, in both cases, there are difficulties with intermediate steps, such as eliminating hydrogens in a H-rich gas and rearranging bonds in a closed carbon cage.[1] Furthermore, ultraviolet (UV) radiation is often required for these processes, and some evolved stars which are sources of C_{60}, such as IRAS 06338, are too cool to be substantial UV emitters (e.g., refs 14 and 15).

Recently, Bernal et al.[16] conducted laboratory experiments showing that C_{60} can arise from rapid heating of silicon carbide (SiC) grains with a 3C-cubic structure. Such SiC grains are commonly produced in the circumstellar envelopes of carbon-rich Asymptotic Giant Branch (AGB) stars, as infrared observations of the 11.3 μm Si−C stretch have clearly

Received: February 28, 2022
Revised: June 12, 2022

demonstrated (e.g., ref 17). Furthermore, studies of presolar SiC grains extracted from meteorites show that 80% of them have the 3C-cubic structure.[18,19] Once SiC grains are formed in circumstellar gas, they can be heated by shocks either in the late, thermal-pulsing (TP) stage on the AGB, or in the protoplanetary nebula (PPN) phase, where extreme mass loss occurs at high velocities (>100 km s^{-1}: e.g., ref 20). Also, stellar radiation may heat the grains as the white dwarf stage is approached. Simulating these energetic circumstellar environments, Bernal et al.[16] showed that when analog grains undergo rapid heating to ∼1300 K, along with ion bombardment (150 keV Xe), silicon is leached from the grain surface, creating layered graphitic sheets. Using transmission electron microscopy (TEM) imaging and spectroscopy, surface defects in the crystal were found to distort the six-membered rings characteristic of graphite, creating hemispherical structures with the necessary 5-membered rings and diameters matching that of C_{60}. These experiments suggest an alternate route for synthesizing C_{60} and possibly other fullerene structures such as carbon nanotubes.

In order to further explore the synthesis of fullerenes from SiC grains, we have conducted additional TEM experiments using a different heating rate from the Bernal et al.[16] publication and without high energy ion bombardment. Previous work has demonstrated that carbon nanotubes (CNTs) can form from SiC decomposition,[21,22] and so experiments with higher temperatures were a natural follow-up to our previous effort. In this paper, we present our new results: the first measurements of multiwalled carbon nanotubes (MWCNTs) formed via thermal decomposition of analog, presolar grain-sized SiC. High-resolution TEM instrumentation was used to heat and image analog SiC grains in situ and characterize the resulting synthesized nanostructures. The dimensions of the formed nanostructures (including the lattice spacing of the nanotube walls) were measured in several locations. Post-mortem TEM images of the heated SiC samples were also obtained. We also discuss their implications for the presence of C_{60} and carbon nanotubes in the ISM.

EXPERIMENTAL METHODS

For in situ heating experiments, we used the Hitachi HF5000 scanning transmission electron microscope (S/TEM) located in the Kuiper Materials Imaging and Characterization Facility at the Lunar and Planetary Laboratory, University of Arizona. The HF5000 is equipped with a cold-field emission gun, a third-order spherical-aberration corrector for STEM mode, bright-field (BF), dark-field (DF), and secondary electron STEM detectors, and an Oxford Instruments X-Max N 100 TLE EDS system with dual 100 mm^2 windowless silicon-drift detectors providing a large solid angle (Ω = 2.0 sr) for rapid EDS mapping of samples in minutes instead of hours. It is also equipped with a Gatan OneView 4k × 4k pixel CMOS camera for the acquisition of TEM images and electron-diffraction patterns. The HF5000 has a spatial resolution of 0.23 nm in TEM mode (parallel illumination) and 0.078 nm for scanning mode (converged beam). The HF5000 has the capability of using either 200 or 60 keV alignments, and the 200 keV alignment was used in this experiment because of the higher imaging resolution.

A 3C-SiC sample (U.S. Research Nanomaterials) was obtained, the same crystal polytype as is common in presolar SiC grains, as mentioned.[18,19] A dispersion of the SiC sample and methanol was prepared and deposited on a microelectromechanical systems (MEMS) chip manufactured by Norcada (Model HTN-0101H) to achieve a monodispersion of grains on the support film. Once suitably prepared, the chip was loaded into the Hitachi "Blaze" TEM holder for in situ heating. The MEMS chip consists of SiN membranes that sandwich a heating element, which is manufactured by Norcada (https://www.norcada.com/products/nitride-windows-tem/). A controller box powers the MEMS chip, which is operated through a Labview interface. Variable ramp rates, set points, and isothermal holds are achievable with the Blaze holder and MEMS platform. The chip itself has a temperature limit of 1100 °C, above which the SiN membrane will thermally degrade to failure, resulting in breakage of the film and catastrophic loss of the sample. Isothermal holds at 1100 °C are possible but can only be performed for short durations, and extended experiments at this temperature are generally avoided. In comparison, isothermal holds slightly below the upper temperature limit are stable for extended periods of time. The MEMS chip can also rapidly cool to a desired temperature (as low as ambient temperature) by TEM computer control.

Two heating experiments were performed. For both experiments, a region with several SiC crystals was imaged until the temperature reached ∼1050 °C, after which other positions with additional SiC grains were observed. The first experiment was conducted over ∼4.5 h. The SiC sample was inserted into the TEM at room temperature for ∼1 h during which time we aligned the microscope, searched for suitable areas to monitor during the experiment, and acquired images for baseline reference. We located several areas of the sample that provided suitable monodispersed grains for in situ monitoring, and we stored those stage positions to aid in rapid switching of imaging locations on the MEMS chip during the experiment. The sample was then heated from room temperature to 800 °C over 30 min (∼25.7 °C/min). This temperature and ramp rate were chosen to evaporate any potential contamination from organic solvents that might still be present on the sample surface. The sample temperature was then increased to 1050 °C over 1 h (∼4.2 °C/min). This heating rate was used because previous work suggests that a slower rate is more likely to form carbon nanobuds rather than graphene sheets, which prefer more rapid warming.[23] Once the set point temperature of 1050 °C was reached, we held the sample isothermally at 1050 °C for a period of 13 min. We performed a second experiment to verify our results. This second experiment was similar to the first, in which we inserted the SiC sample, aligned the TEM, imaged several SiC grains monodispersed on the SiN film, and chose a suitable region to image during heating. The sample was first heated to 800 °C at a ramp rate of ∼25.7 °C/min, then heated to 1050 °C at a ramp rate of ∼4.2 °C/min. After reaching the programmed temperature of 1050 °C, the sample was held isothermally for 3 h. In both experiments, the sample temperature was cooled at a rate of −17.0 degrees per minute to ambient temperature. Images and video were acquired on the initial SiC sample, then both during and after the heating.

RESULTS

SiC is stable at ambient temperature under the electron beam. We measured the sample prior to experiments, and both selected-area electron diffraction patterns and EDS mapping reveal sample homogeneity and crystallinity. Prior to heating, we surveyed the grain distribution on the SiN membrane. At

https://doi.org/10.1021/acs.jpca.2c01441
J. Phys. Chem. A XXXX, XXX, XXX−XXX

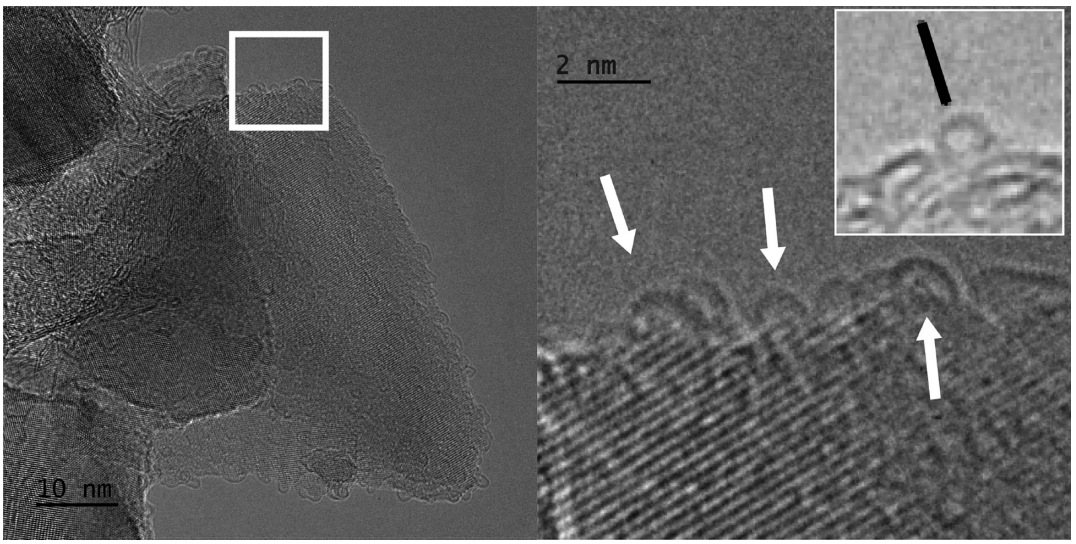

Figure 1. (Left) HRTEM image of a SiC sample grain acquired at 1050 °C (experiment 2), with fullerene-sized hemispheres coating the surface. (Right) Enlarged image of the region bounded by white rectangle in left image. Hemispherical structures ∼1 nm diameter are indicated by white arrows. The inset shows a state-of-the-art TEM image of C_{60}, indicated by a black line, reproduced with permission from ref 24. Copyright 2004 Elsevier. Note that the image here and that of ref 24 are virtually identical.

∼1000 °C, we observed the grain surface changing from the SiC crystal structure to exhibiting an increasingly graphitic structure. We note that the SiN membrane of the MEMS chip expands in the Z dimension during heating, making it challenging to image at the eucentric position over the field of view.

As the temperature approached 1050 °C, small hemispherical structures with the approximate size of C_{60} (∼1 nm) were initially observed on the grain surface in both experiments. These data confirm our previous results and are consistent with the formation of C_{60} from the grains (see, e.g., ref 24). Note that it is extremely difficult to view individual C_{60} molecules with TEM, and our images are virtually identical to other TEM measurements of this species aimed solely at obtaining its detection.[24] The appearance of round nanobuds over the entire crystal surface is illustrated in Figure 1. This figure presents a TEM image of C_{60}-sized hemispherical structures on the surface of a crystal (experiment 2), as the SiC began to reach 1050 °C. The inset shows a state-of-the-art C_{60} image from HRTEM, for comparison.

We subsequently observed the formation of surficial nanostructures, which increased in size with multiple curved layers, separated ∼0.36 nm apart, indicative of graphitic carbon in the form of MWCNTs.[25] Figure 2 provides a TEM image of the small SiC grain (experiment 1) with the curved MWCNT coating. The inset shows a TEM image of a MWCNT displayed for comparison.[26]

As the heating duration progressed in both experiments, the structures on the SiC grain became increasingly ordered, with the clear appearance of nanotubes. The structures contained several graphene layers with curvature and dimensions indicating a tubular form. Figure 3 provides a TEM image of a region with SiC particles coated with MWCNTs (experiment 2). Figure 4 provides enlarged images of the MWCNTs from Figures 2 and 3. The observed graphene layers and nanostructures were measurably larger (>3 nm vs the initial ∼1 nm of the nanobuds) as heating duration increased, several graphitic layers appeared to roll onto themselves. It is possible in our experiments that the imaging electron beam provides some additional heat, which aids nanostructure formation; however, this temperature contribution is negligible in comparison to that of the MEMS heating apparatus.

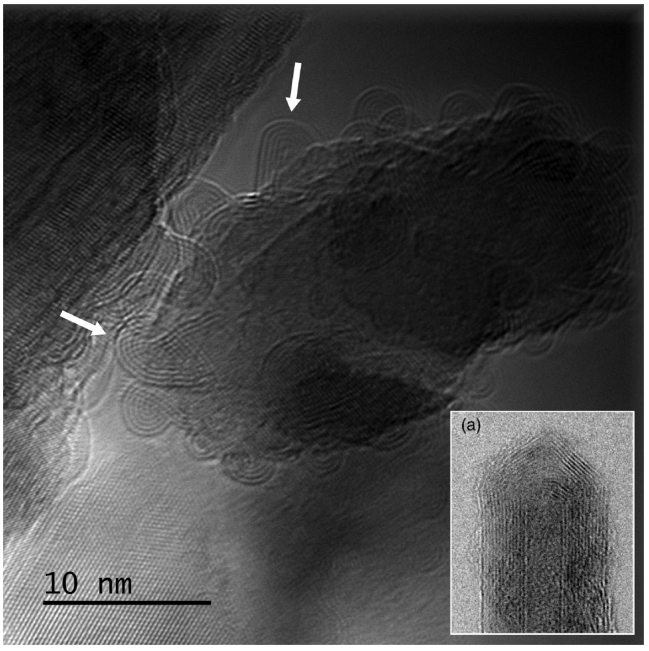

Figure 2. High-resolution TEM image of a 3C-SiC sample grain (center) acquired at 1050 °C (experiment 1). The surface of the grain has a surface coated with MWCNTs, indicated by white arrows. The MWCNTs are several nm in length/width. The inset shows a state-of-the-art TEM image of a MWCNT (approximately 10 nm in diameter), reproduced with permission from ref 26. Copyright 2012 American Physical Society. The similarity is striking.

After heating was concluded in experiment 1, the sample temperature was decreased to 30 °C. The MWCNTs remained intact on the SiC sample surface. Approximately 9 days later, we performed postheating characterization at room temperature but noticed that the MWCNTs were absent from surface

https://doi.org/10.1021/acs.jpca.2c01441
J. Phys. Chem. A XXXX, XXX, XXX−XXX

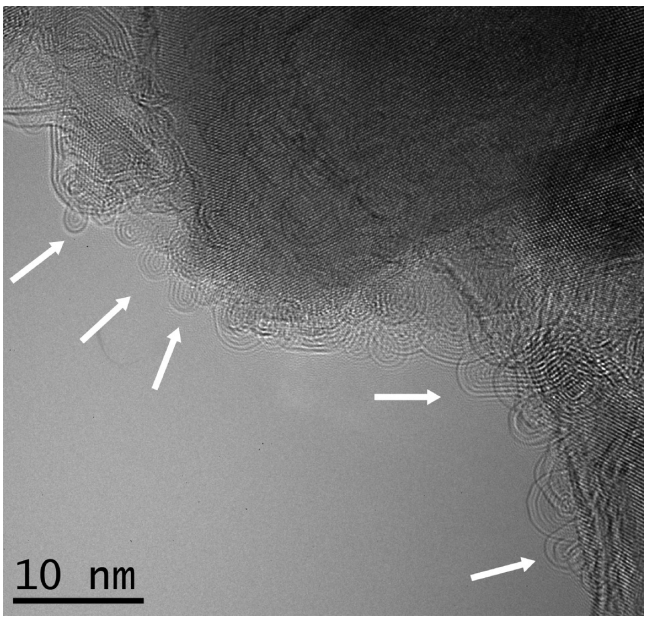

Figure 3. High-resolution TEM image of 3C-SiC sample grains acquired at 1050 °C (experiment 2). The surface of the SiC particle is now coated with MWCNTs, indicated by white arrows. As with experiment 1, the imaged MWCNTs are several nm in length/width.

locations where they had previously been observed. Also, the SiC grains had a noticeable decline in the size of the crystal.

Figure 5 shows TEM images of a SiC sample before and after prolonged MEMS heating. Experiment 2 reproduced similar nanostructures as in the first experiment, where MWCNTs coated the SiC sample (Figures 2, 3, and 4). After the sample was cooled to ambient, the MWCNT coating decreased in size and order, suggesting both amorphization and removal of material occurred under prolonged exposure to the electron beam.

DISCUSSION

The synthesis of carbon nanostructures via thermal decomposition of SiC (including the 3-C polytype used in this experiment) is a well-documented phenomenon (see, e.g., refs 27, 21, and 28). During the initial thermal decomposition, the silicon vapor pressure exceeds that of carbon.[29] Si atoms consequently leach from the SiC crystal, leaving a residual layer of epitaxial graphene for every three SiC bilayers decomposed via this process. Because the graphene growth depends on sublimation of Si from the crystal, the pressure conditions surrounding the crystal affect the growth rate, quality, and initial growth temperature of the epitaxial graphene. Ultrahigh vacuum (UHV) conditions provide a faster graphene growth rate at the expense of lower graphene quality,[29] while higher pressures (in an argon environment) provide slower growth and higher graphene quality.[30] However, studies of SiC thermal decomposition are typically concerned with electronics manufacturing, which uses chemically etched wafers with as few surface defects as possible in pressure conditions ranging from atmospheric to UHV.[28] In comparison, the few available studies of SiC thermal decomposition in which defects occur on the surface show that they aid in the formation of graphene layers.[28,31]

At higher temperatures, SiC can continue to decompose past the formation of epitaxial graphene, with transformation of the graphene layers into carbon nanobuds/nanocaps. During the initial formation of carbon nanobuds, the epitaxial graphene layer undergoes a distortion, where the initial six-membered rings of the graphene are rearranged into five-membered rings at the area of nanobud curvature and seven-membered rings at the nanobud/graphene layer interface.[22] The initial nanobuds have approximately the diameter of C_{60}[22,16] and, to the limit of measurement techniques, are indeed this molecule. Nanobuds form via SiC decomposition in conditions including ultrahigh vacuum (UHV), O_2, and H_2 atmospheres.[23,32,33]

In the final phase of SiC thermal decomposition, the previously formed carbon nanobuds act as nucleation sites and grow into carbon nanotubes (CNTs).[22] Graphene layers which have at this point formed below the surface layer distort, creating multiwalled tubes. Note that the previous nanobuds are single-walled. The CNTs, like the nanobuds they formed from, grow perpendicular to the SiC crystal surface. CNTs formed via this process are capped on the ends and exhibit the

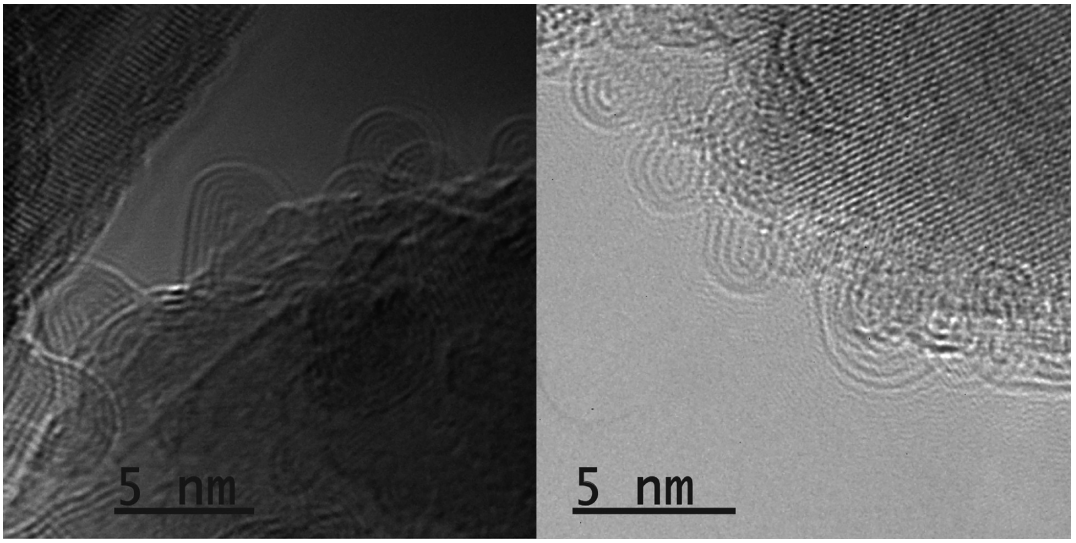

Figure 4. (Left) Enlarged image of select MWCNTs from Figure 1 (experiment 1). (Right) Enlarged image of select MWCNTs from Figure 3 (experiment 2).

https://doi.org/10.1021/acs.jpca.2c01441
J. Phys. Chem. A XXXX, XXX, XXX−XXX

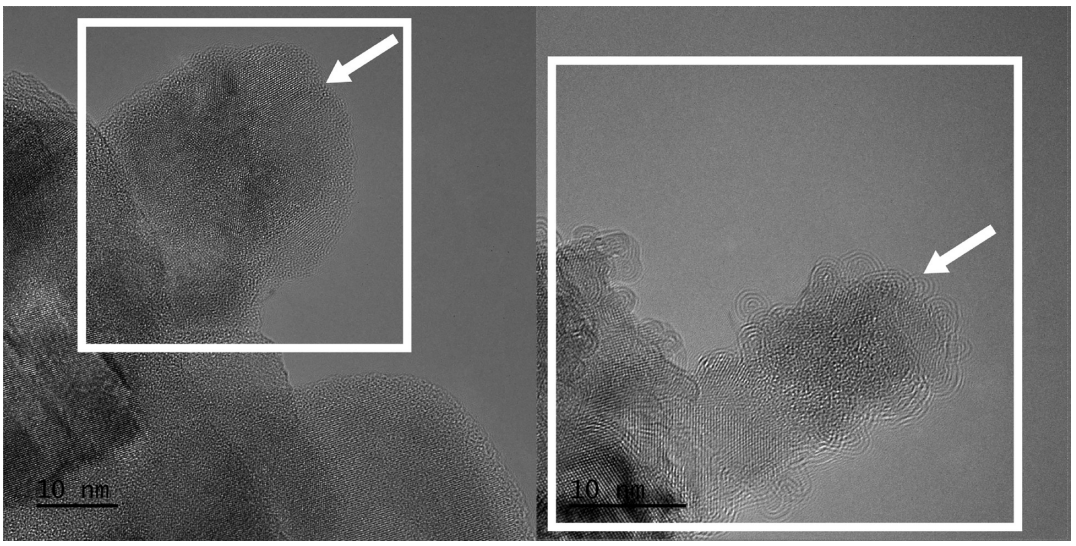

Figure 5. (Left) SiC grain before MEMS heating, indicated by a white arrow (experiment 2). (Right) The same SiC grain imaged during MEMS heating at 1050 °C, indicated by a white arrow. The dimensions of the SiC sample rapidly diminished at 1050 °C. The white squares in each panel represent the same area dimension.

"zigzag" chirality.[34] Prior experimental studies of CNT formation typically use chemically etched SiC wafers, as epitaxial nanotubes are of interest in electronics manufacturing.[21,22]

Our experiment analyzed this thermal decomposition process on smaller SiC crystals than those used in prior studies. Our smaller crystals have more surface curvature, which appears to aid in the distortion of formed graphene, preferentially creating CNTs on the surface. The CNTs formed in this experiment are shorter in length than those formed by Kusunoki et al.[21] (~4 nm vs ~12 nm); however, that experiment used YAG laser heating and achieved higher temperatures than the capabilities of our MEMS chip (1700 °C vs ~1100 °C). This previous work suggests that higher temperatures may form even larger CNTs than observed in this study. Also, the MWCNT formation was not seen in the work of Bernal et al.,[16] where 150 keV Xe bombardment and heating to 1000 °C was used. Under the vacuum conditions of the HF5000, CNT formation occurs above 1000 °C, and prolonged heating above this threshold forms larger, increasingly ordered structures.

Refractory grains are well-known to condense out of the hot gas near the stellar photosphere during mass loss in evolved stars, primarily on the AGB but also in very massive, hypergiant stars (e.g., refs 20 and 37). SiC grains are commonly formed in carbon-rich circumstellar envelopes, as supported by observations[17] and meteorite studies of presolar grains.[18] Such grains can experience destructive processing on the latter part of the AGB, when thermal pulses, created by helium-shell flashes, generate shock waves in the extended stellar atmosphere which propagate into the envelope.[38] Further grain processing occurs in the PPNe phase, when much faster winds impact the slower moving remnant AGB shell, with velocities ~100−200 km s^{-1}.[39] Also, the stellar temperature increases for PPNe, generating significant UV radiation which may also thermally process the grains. Toward PPNe, the $v = 1-0$ vibrationally excited lines of H_2 near 2 μm were observed, which are clear shock indicators.[40] These lines are not observed in AGB stars but become visible in the PPNe phase. The presence of vibrationally excited H_2 indicates gas with $T \sim 1000-2000$ K (e.g., ref 41), comparable to what is achieved in the lab experiments. Such shocks can also include the impact and implantation of ions onto grain surfaces (e.g., refs 42 and 43). Dust temperatures of ~1200−1600 K have been observed in TP-AGB stars, post-AGB objects, and planetary nebulae (e.g., refs 44−47). In these sources, the hot dust components are thought to arise from recent, energetic mass loss, an inherently nonequilibrium process, such that equilibrium cooling has not yet been achieved.

The largest currently known interstellar molecules are the fullerenes C_{60} and C_{70}. While C_{60} is comprised of 60 carbon atoms, its diameter is 0.7 nm.[24] The MWCNT structures formed in this experiment, several times the size of C_{60} and with multiple walls, may easily exceed 1000 carbon atoms. Because SiC is a common solid-state circumstellar material, verified by decades of both mm-wave/IR astronomy and present as presolar grains in meteoritic material, any organic molecules formed epitaxially on the surface is a major concern to understanding chemical complexity in the ISM. Figure 6

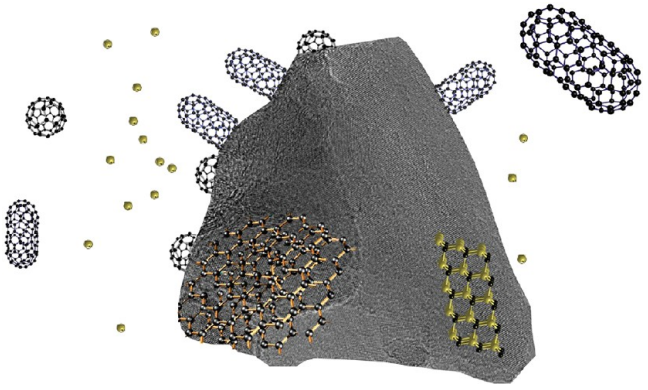

Figure 6. Illustration of relevant nanostructures that may populate the ISM, starting with 3C-SiC, leading to graphene, C_{60}, and CNTs. Image adapted with permission from this work, ref 16, ref 35, and ref 36. Copyright 2022 American Chemical Society, copyright 2019 American Astronomical Society, copyright 2015 Wiley-VCH, and copyright 2002 Royal Society of Chemistry, respectively.

https://doi.org/10.1021/acs.jpca.2c01441
J. Phys. Chem. A XXXX, XXX, XXX−XXX

provides a cartoon illustration of the relevant nanostructures that might populate the ISM, also observed in these experiments. Carbon nanotubes are known to have high stability to radiation, and fullerenes are able to survive for potentially Gyr time scales when adequately shielded.[48,49]

After the discovery of interstellar C_{60}, other fullerenic molecules were proposed as additional DIB carriers.[50] One theory for the DIB carriers are large carbonaceous molecules with high stability under interstellar conditions.[50] Carbon nanotubes are known for near-perfect optical absorption properties and are used to create some of the darkest synthetic materials.[51] CNTs also have long lifetimes in high-radiation environments,[48] as mentioned, making them excellent candidate carriers of the diffuse interstellar bands (DIBs).[52] Of these hundreds of unassigned DIB absorption features, a few have been attributed to C_{60}^+,[6] which we also have proposed is possibly formed by SiC thermal decomposition.[16] Planetary nebulae are responsible for the majority (∼80%) of material ejected into diffuse gas, linking the post-AGB environment to the DIBs.[53]

CONCLUSIONS

Presolar SiC grain analogs with the 3C polytype were heated in situ and characterized by high-resolution TEM. Both "buckyball" structures and MWCNTs were synthesized via thermal decomposition of the SiC sample and imaged. The resulting MWCNTs exhibited sizes of ∼3 to 4 nm in length, and ∼3 to 4 nm in width, larger in size than buckminsterfullerene (C_{60}). The largest imaged MWCNTs are comprised of >4 layers of graphitic carbon, with a lattice spacing of ∼0.36 nm. These nanostructures are estimated to contain over a thousand carbon atoms and were found to be removable from the SiC sample surface. We hypothesize fullerenes, nanotubes, and other nanostructures are likely formed by heating circumstellar SiC dust in post-AGB environments and then survive injection into the ISM through the PN phase. These structures have a strong possibility of being responsible for the many unidentified diffuse interstellar bands (DIBs) and may contain a significant fraction of the interstellar carbon.

AUTHOR INFORMATION

Corresponding Author

Jacob J. Bernal − *Lunar and Planetary Laboratory, University of Arizona, Tucson, Arizona 85721, United States;* orcid.org/0000-0001-6176-0773; Email: jjbernal1@email.arizona.edu

Authors

Thomas J. Zega − *Lunar and Planetary Laboratory, University of Arizona, Tucson, Arizona 85721, United States; Department of Materials Science and Engineering, University of Arizona, Tucson, Arizona 85721, United States*

Lucy M. Ziurys − *Departments of Astronomy and Chemistry, University of Arizona, Tucson, Arizona 85721, United States*

Complete contact information is available at: https://pubs.acs.org/10.1021/acs.jpca.2c01441

Notes

The authors declare no competing financial interest.

ACKNOWLEDGMENTS

This work is supported by the National Science Foundation MPS-Ascend Postdoctoral Research Fellowship under Grant AST-2137919, NSF Grant AST-1907910, NASA Grant 80NSSC19K0509 and NASA Grant 80NSSC21K0593 ("Alien Earths"). We acknowledge NASA grants #NNX12AL47G and #NNX15AJ22G, and 0619599 for funding of the instrumentation in the Kuiper Materials Imaging and Characterization Facility at the Lunar and Planetary Laboratory, University of Arizona. We thank Dr. Jerry Chang at the Kuiper Materials Imaging and Characterization Facility at the Lunar and Planetary Laboratory, University of Arizona, for help with analyzing the samples.

REFERENCES

(1) Omont, A.; Bettinger, H. F. Intermediate-Size Fullerenes as Degradation Products of Interstellar Polycyclic Aromatic Hydrocarbons. *Astron. Astrophys.* **2021**, *650*, A193.

(2) Cami, J.; Bernard-Salas, J.; Peeters, E.; Malek, S. E. Fullerenes in Circumstellar and Interstellar Environments. *Proc. Int. Astron. Union* **2011**, *7* (S280), 216−227.

(3) Zhang, Y.; Kwok, S. Detection of C_{60} in the Protoplanetary Nebula IRAS 01005 + 7910. *Astrophys. J.* **2011**, *730* (2), 126.

(4) Zhang, Y.; Kwok, S.; Sadjadi, S. Fullerenes and Fulleranes in Circumstellar Envelopes. *J. Phys. Conf. Ser.* **2016**, *728*, 052004.

(5) Berné, O.; Cox, N. L. J.; Mulas, G.; Joblin, C. Detection of Buckminsterfullerene Emission in the Diffuse Interstellar Medium. *Astron. Astrophys.* **2017**, *605*, L1.

(6) Campbell, E. K.; Holz, M.; Gerlich, D.; Maier, J. P. Laboratory Confirmation of C_{60}^+ as the Carrier of Two Diffuse Interstellar Bands. *Nature* **2015**, *523* (7560), 322−323.

(7) Walker, G. A. H.; Bohlender, D. A.; Maier, J. P.; Campbell, E. K. IDENTIFICATION OF MORE INTERSTELLAR C_{60}^+ BANDS. *Astrophys. J. Lett.* **2015**, *812* (1), L8.

(8) Cordiner, M. A.; Linnartz, H.; Cox, N. L. J.; Cami, J.; Najarro, F.; Proffitt, C. R.; Lallement, R.; Ehrenfreund, P.; Foing, B. H.; Gull, T. R.; et al. Confirming interstellar C_{60}^+ using the Hubble space telescope. *Astrophys. J. Lett.* **2019**, *875* (2), L28.

(9) Berné, O.; Tielens, A. G. G. M. Formation of Buckminsterfullerene (C_{60}) in Interstellar Space. *Proc. Natl. Acad. Sci. U. S. A.* **2012**, *109* (2), 401−406.

(10) Duley, W. W.; Hu, A. Fullerenes and Proto-Fullerenes in Interstellar Carbon Dust. *Astrophys. J. Lett.* **2012**, *745*, L11.

(11) Carpentier, Y.; Féraud, G.; Dartois, E.; Brunetto, R.; Charon, E.; Cao, A.-T.; d'Hendecourt, L.; Bréchignac, P.; Rouzaud, J.-N.; Pino, T. Nanostructuration of Carbonaceous Dust as Seen through the Positions of the 6.2 and 7.7μm AIBs. *Astron. Astrophys.* **2012**, *548*, A40.

(12) Zhang, W.; Si, Y.; Zhen, J.; Chen, T.; Linnartz, H.; Tielens, A. G. G. M. Laboratory Photochemistry of Covalently Bonded Fluorene Clusters: Observation of an Interesting PAH Bowl-Forming Mechanism. *Astrophys. J.* **2019**, *872* (1), 38.

(13) Berné, O.; Montillaud, J.; Joblin, C. Top-down formation of fullerenes in the interstellar medium. *Astron. Astrophys.* **2015**, *577*, A133.

(14) Zhang, Y.; Kwok, S. On the Detections of C_{60} and Derivatives in Circumstellar Environments. *Earth Planets Space* **2013**, *65* (10), 1069−1081.

(15) Gielen, C.; Cami, J.; Bouwman, J.; Peeters, E.; Min, M. Carbonaceous Molecules in the Oxygen-Rich Circumstellar Environment of Binary Post-AGB Stars: C_{60} fullerenes and Polycyclic Aromatic Hydrocarbons. *Astron. Astrophys.* **2011**, *536*, A54.

(16) Bernal, J. J.; Haenecour, P.; Howe, J.; Zega, T. J.; Amari, S.; Ziurys, L. M. Formation of Interstellar C_{60} from Silicon Carbide Circumstellar Grains. *Astrophys. J. Lett.* **2019**, *883* (2), L43.

(17) Kwok, S. The Synthesis of Organic and Inorganic Compounds in Evolved Stars. *Nature* **2004**, *430* (7003), 985−991.

(18) Daulton, T. L.; Bernatowicz, T. J.; Lewis, R. S.; Messenger, S.; Stadermann, F. J.; Amari, S. Polytype Distribution in Circumstellar Silicon Carbide. *Science* **2002**, *296* (5574), 1852−1855.
(19) Daulton, T. L.; Bernatowicz, T. J.; Lewis, R. S.; Messenger, S.; Stadermann, F. J.; Amari, S. Polytype Distribution of Circumstellar Silicon Carbide. *Geochim. Cosmochim. Acta* **2003**, *67* (24), 4743−4767.
(20) Van Winckel, H. Post-AGB Stars. *Annu. Rev. Astron. Astrophys.* **2003**, *41* (1), 391−427.
(21) Kusunoki, M.; Rokkaku, M.; Suzuki, T. Epitaxial Carbon Nanotube Film Self-Organized by Sublimation Decomposition of Silicon Carbide. *Appl. Phys. Lett.* **1997**, *71* (18), 2620−2622.
(22) Watanabe, H.; Hisada, Y.; Mukainakano, S.; Tanaka, N. In Situ Observation of the Initial Growth Process of Carbon Nanotubes by Time-Resolved High Resolution Transmission Electron Microscopy. *J. Microsc.* **2001**, *203* (1), 40−46.
(23) Maruyama, T.; Naritsuka, S. Initial Growth Process of Carbon Nanotubes in Surface Decomposition of SiC. In *Carbon Nanotubes - Synthesis, Characterization, Applications*, Yellampalli, S., Ed.; IntechOpen, 2011, DOI: 10.5772/17253.
(24) Goel, A.; Howard, J. B.; Vander Sande, J. B. Size Analysis of Single Fullerene Molecules by Electron Microscopy. *Carbon N. Y.* **2004**, *42* (10), 1907−1915.
(25) Sakharova, N. A.; Pereira, A. F. G.; Antunes, J. M.; Fernandes, J. V. Mechanical Characterization of Multiwalled Carbon Nanotubes: Numerical Simulation Study. *Materials (Basel)* **2020**, *13* (19), 4283.
(26) Heeres, E. C.; Oosterkamp, T. H.; de Jonge, N. Size of the Localized Electron Emission Sites on a Closed Multiwalled Carbon Nanotube. *Phys. Rev. Lett.* **2012**, *108* (3), 036804.
(27) Van Bommel, A. J.; Crombeen, J. E.; Van Tooren, A. LEED and Auger Electron Observations of the SiC(0001) Surface. *Surf. Sci.* **1975**, *48* (2), 463−472.
(28) Mishra, N.; Boeckl, J.; Motta, N.; Iacopi, F. Graphene Growth on Silicon Carbide: A Review: Graphene Growth on Silicon Carbide. *Phys. Status Solidi (a)* **2016**, *213* (9), 2277−2289.
(29) de Heer, W. A.; Berger, C.; Ruan, M.; Sprinkle, M.; Li, X.; Hu, Y.; Zhang, B.; Hankinson, J.; Conrad, E. Large Area and Structured Epitaxial Graphene Produced by Confinement Controlled Sublimation of Silicon Carbide. *Proc. Natl. Acad. Sci. U. S. A.* **2011**, *108* (41), 16900−16905.
(30) Emtsev, K. V.; Bostwick, A.; Horn, K.; Jobst, J.; Kellogg, G. L.; Ley, L.; McChesney, J. L.; Ohta, T.; Reshanov, S. A.; Röhrl, J.; et al. Towards Wafer-Size Graphene Layers by Atmospheric Pressure Graphitization of Silicon Carbide. *Nat. Mater.* **2009**, *8* (3), 203−207.
(31) Hite, J. K.; Twigg, M. E.; Tedesco, J. L.; Friedman, A. L.; Myers-Ward, R. L.; Eddy, C. R.; Gaskill, D. K. Epitaxial Graphene Nucleation on C-Face Silicon Carbide. *Nano Lett.* **2011**, *11* (3), 1190−1194.
(32) Ueda, K.; Iijima, Y.; Maruyama, T.; Naritsuka, S. Effect of Annealing in Hydrogen Atmosphere on Carbon Nanocap Formation in Surface Decomposition of 6H-SiC(000−1). *J. Nanosci. Nanotechnol.* **2010**, *10* (6), 4054−4059.
(33) Maruyama, T.; Bang, H.; Fujita, N.; Kawamura, Y.; Naritsuka, S.; Kusunoki, M. STM and XPS studies of early stages of carbon nanotube growth by surface decomposition of 6H−SiC(000−1) under various oxygen pressures. *Diamond Relat. Mater.* **2007**, *16* (4−7), 1078−1081.
(34) Kusunoki, M.; Suzuki, T.; Honjo, C.; Hirayama, T.; Shibata, N. Selective synthesis of zigzag-type aligned carbon nanotubes on SiC (000−1) wafers. *Chem. Phys. Lett.* **2002**, *366* (5−6), 458−462.
(35) Carbone, M.; Gorton, L.; Antiochia, R. An Overview of the Latest Graphene-Based Sensors for Glucose Detection: The Effects of Graphene Defects. *Electroanalysis* **2015**, *27* (1), 16−31.
(36) Silver, T.; Pan, A. V.; Ionescu, M.; Qin, M. J.; Dou, S. X. 9 Developments in High Temperature Superconductivity. *Annu. Rep. Sect. C (Phys. Chem.)* **2002**, *98* (0), 323−373.
(37) O'Gorman, E.; Vlemmings, W.; Richards, A. M. S.; Baudry, A.; De Beck, E.; Decin, L.; Harper, G. M.; Humphreys, E. M.; Kervella, P.; Khouri, T.; et al. ALMA Observations of Anisotropic Dust Mass Loss in the Inner Circumstellar Environment of the Red Supergiant VY Canis Majoris. *Astron. Astrophys.* **2015**, *573*, L1.
(38) Höfner, S.; Olofsson, H. Mass Loss of Stars on the Asymptotic Giant Branch: Mechanisms, Models and Measurements. *Astron. Astrophys. Rev.* **2018**, *26* (1), DOI: DOI: 10.1007/s00159-017-0106-5.
(39) Davis, C. J.; Smith, M. D.; Gledhill, T. M.; Varricatt, W. P. Near-Infrared Echelle Spectroscopy of Protoplanetary Nebulae: Probing the Fast Wind in H2. *Mon. Not. R. Astron. Soc.* **2005**, *360* (1), 104−118.
(40) Van Winckel, H. Why Is the Red Rectangle Unique? *Proc. Int. Astron. Union* **2013**, *9* (S297), 180−186.
(41) Bujarrabal, V.; Alcolea, J.; Neri, R. The Structure and Dynamics of the Proto−Planetary Nebula M1−92. *Astrophys. J.* **1998**, *504* (2), 915−920.
(42) Heck, P. R.; Amari, S.; Hoppe, P.; Baur, H.; Lewis, R. S.; Wieler, R. Ne ISOTOPES IN INDIVIDUAL PRESOLAR GRAPHITE GRAINS FROM THE MURCHISON METEORITE TOGETHER WITH He, C, O, Mg-Al ISOTOPIC ANALYSES AS TRACERS OF THEIR ORIGINS. *Astrophys. J.* **2009**, *701* (2), 1415−1425.
(43) Verchovsky, A. B.; Wright, I. P.; Pillinger, C. T. Astrophysical Significance of Asymptotic Giant Branch Stellar Wind Energies Recorded in Meteoritic SiC Grains. *Astrophys. J.* **2004**, *607* (1), 611−619.
(44) Waters, L. B. F. M.; Sahu, K. C. Post-AGB Candidates. *Symposium* **1993**, *155*, 271−278.
(45) Rudy, R. J.; Lynch, D. K.; Mazuk, S.; Puetter, R. C.; Dearborn, D. S. P. The Near-Infrared Spectrum of the Planetary Nebula IC 5117. *Astron. J.* **2001**, *121* (1), 362−370.
(46) Nanni, A.; Marigo, P.; Groenewegen, M. A. T.; Aringer, B.; Girardi, L.; Pastorelli, G.; Bressan, A.; Bladh, S. Constraining Dust Properties in Circumstellar Envelopes of C-Stars in the Small Magellanic Cloud: Optical Constants and Grain Size of Carbon Dust. *Mon. Not. R. Astron. Soc.* **2016**, *462* (2), 1215−1237.
(47) Lagadec, E.; Mékarnia, D.; de Freitas Pacheco, J. A.; Dougados, C. Dust Temperature and Density Profiles in the Envelopes of AGB and Post-AGB Carbon Stars from Mid-Infrared Observations. *Astron. Astrophys.* **2005**, *433* (2), 553−564.
(48) Li, B.; Feng, Y.; Ding, K.; Qian, G.; Zhang, X.; Zhang, J. The Effect of Gamma Ray Irradiation on the Structure of Graphite and Multi-Walled Carbon Nanotubes. *Carbon N. Y.* **2013**, *60*, 186−192.
(49) Cataldo, F.; Strazzulla, G.; Iglesias-Groth, S. Stability of C_{60} and C_{70} fullerenes toward Corpuscular and γ Radiation. *Mon. Not. R. Astron. Soc.* **2009**, *394* (2), 615−623.
(50) Omont, A. Interstellar Fullerene Compounds and Diffuse Interstellar Bands. *Astron. Astrophys.* **2016**, *590*, A52.
(51) Yang, Z.-P.; Ci, L.; Bur, J. A.; Lin, S.-Y.; Ajayan, P. M. Experimental Observation of an Extremely Dark Material Made by a Low-Density Nanotube Array. *Nano Lett.* **2008**, *8* (2), 446−451.
(52) Zhou, Z.; Sfeir, M. Y.; Zhang, L.; Hybertsen, M. S.; Steigerwald, M.; Brus, L. Graphite, tubular PAHs, and the diffuse interstellar bands. *Astrophys. J.* **2006**, *638* (2), L105−L108.
(53) Dorschner, J.; Henning, T. Dust Metamorphosis in the Galaxy. *Astron. Astrophys. Rev.* **1995**, *6* (4), 271−333.

https://doi.org/10.1021/acs.jpca.2c01441
J. Phys. Chem. A XXXX, XXX, XXX−XXX